Inorganic Chemistry Communications 155 (2023) 111075

Contents lists available at ScienceDirect

Inorganic Chemistry Communications

journal homepage: www.elsevier.com/locate/inoche

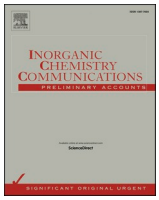

Short communication

Dual S-scheme heterojunction g-C_3N_4/Bi_2S_3/CuS composite with enhanced photocatalytic activity for methyl orange degradation

Damian C. Onwudiwe [a,b,*], Olalekan C. Olatunde [a,b], Violet M. Nkwe [a,b], Youssef Ben Smida [c], Hela Ferjani [d]

[a] Material Science Innovation and Modelling (MaSIM) Research Focus Area, Faculty of Natural and Agricultural Sciences, North-West University, Mafikeng Campus, Private Bag X2046, Mmabatho 2735, South Africa
[b] Department of Chemistry, School of Physical and Chemical Sciences, Faculty of Natural and Agricultural Sciences, North-West University, Mafikeng Campus, Private Bag X2046, Mmabatho 2735, South Africa
[c] University of Carthage, National Center of Materials Sciences Research, Laboratory of Valorization of Useful Materials, Technopole of Borj Cedria, BP 73, 8027 Soliman, Tunisia
[d] Chemistry Department, College of Science, Imam Mohammad Ibn Saud Islamic University (IMSIU), Riyadh 11623, Saudi Arabia

ARTICLE INFO

Keywords:
Redox potential
Charge carriers
Photocatalysis
Heterostructure
Band alignment

ABSTRACT

Weak redox potential and high recombination of charge carriers are two main factors that limit the efficiency of photocatalysts in wastewater treatment. In this study, the synthesis of heterostructure photocatalyst (composed of graphitic carbon nitride, bismuth sulphide, and copper sulphide (g-C_3N_4/Bi_2S_3/CuS)) with improved charge carrier separation and tuned redox potential for improved photocatalysis of methyl orange (MO) dye is reported. The band alignment of the synthesized heterostructure exhibited a synergistic effect, significantly enhancing charge carrier separation and mitigating their recombination. The g-C_3N_4/Bi_2S_3/CuS composite exhibited enhanced photocatalytic efficiency compared to the pristine g-C_3N_4, Bi_2S_3, and CuS. Furthermore, the activity of the heterostructure was observed to increase as the ratio of CuS in the photocatalyst was increased. The highest photocatalytic efficiency was recorded for the g-C_3N_4/Bi_2S_3/CuS(20%), which achieved 98% degradation efficiency and reaction rate constant (k) of 8.08×10^{-2} min^{-1}. Radical scavenging experiments showed that $^{\cdot}OH$, e^-, and h^+ played significant roles in the degradation process. A charge transfer scheme and mechanism of reaction were proposed on this basis.

1. Introduction

Environmental pollution arising from the textile industry has been a serious global problem for many years despite the various environmental regulatory acts [1]. Wastewater from the textile industry contains ~30–40% residual dye, which is discharged into the environment without prior treatment. This waste stream comprises inorganic and organic salts, corrosive acids, and metals which are potential carcinogens and mutagens [2,3]. Methyl orange is a widely used monoazo dye in the textile, chemical, and paint industries. It is associated with several harmful effects such as eye irritation and skin problems [4]. It, therefore, becomes important for this compound to be removed from industrial waste streams before they are discharged into the environment.

Several technologies such as coagulation, adsorption, flocculation, photocatalysis, and ion exchange have been explored for the removal of MO from waste streams. However, most of these techniques suffer from various drawbacks such as high energy consumption, high cost, and production of toxic by-products [5]. Photocatalysis, which is one of the advanced oxidation processes, is a widely used technique for wastewater treatment because of its potential for the degradation of pollutants into harmless final products such as CO_2, H_2O, and inorganic salts [6]. It has proven to be effective in the degradation of several dyes such as Sudan 1 [7], Rhodamine B [8], Bromophenol blue, Eosin Yellow [9], methyl orange [10] and methylene blue [11].

Different classes of semiconductor materials such as metal oxides [12], metal sulphides [13], Mxenes [14], metal–organic frameworks have been explored as photocatalysts in wastewater treatment [15]. Recently, carbon-based materials such as graphene oxide and graphitic

* Corresponding author at: Material Science Innovation and Modelling (MaSIM) Research Focus Area, Faculty of Natural and Agricultural Sciences, North-West University, Mafikeng Campus, Private Bag X2046, Mmabatho 2735, South Africa.
E-mail address: Damian.Onwudiwe@nwu.ac.za (D.C. Onwudiwe).

https://doi.org/10.1016/j.inoche.2023.111075
Received 4 June 2023; Received in revised form 26 June 2023; Accepted 12 July 2023
Available online 13 July 2023

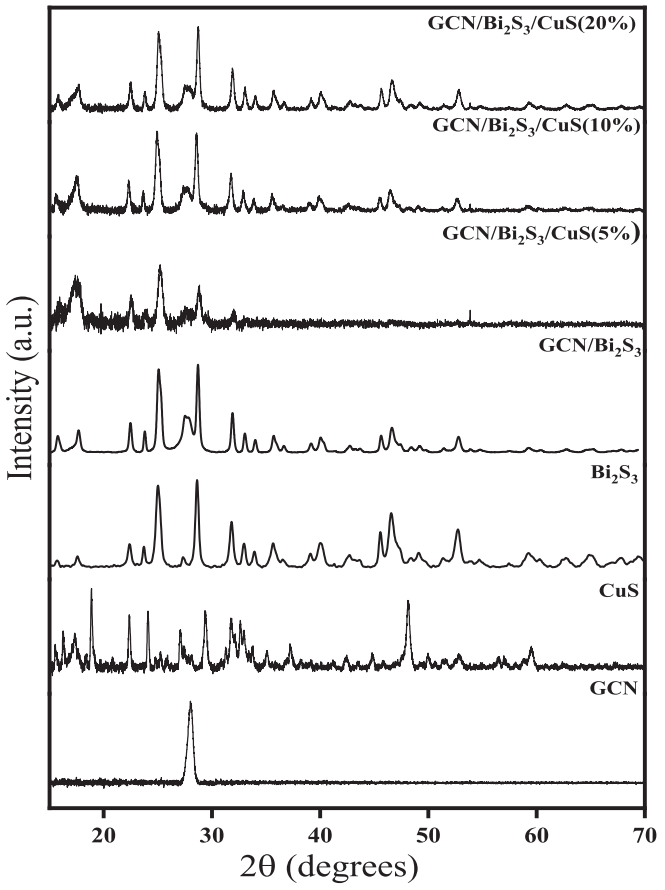

Fig. 1. XRD patterns of GCN, CuS, Bi_2S_3, GCN/Bi_2S_3/CuS (5%), GCN/Bi_2S_3/CuS (10%), and GCN/Bi_2S_3/CuS (20%).

carbon nitrides have also been explored [16]. However, the use of single photocatalytic semiconductor materials is often limited by the band alignment, which results in high recombination of photogenerated charge carriers [17]. Consequently, research focus has shifted to the development of heterostructure photocatalysts, which have proven to be able to mitigate the problem of rapid charge carrier recombination. In addition, heterostructure systems can provide channels for charge carrier transport, which can enhance the photocatalytic performance [18]. Numerous types of heterojunctions such as Z-scheme, type II-scheme and S-scheme heterojunctions have been discovered by the combination of two or more semiconductors [19]. Recent scrutinization of the charge transfer mechanism in the popular Z-scheme and type II has led to the questioning of the plausibility of these mechanisms [20]. This led to the step scheme (S-scheme), which comprises of a reduction photocatalyst (RP) and an oxidation photocatalyst (OP) being proposed.

The fabrication of S-scheme heterostructures has proven effective in enhancing the separation of photogenerated electron-hole pairs [21,22]. An S-scheme heterojunction is comprised of OP and RP with staggered band structures. The photogenerated holes and electrons in the valence band (VB) of OP and conduction band (CB) of RP are preserved, while the unusable charge carriers recombine, leading to a strong redox potential [23]. An upward or downward bending of the band occurs at the semiconductor interface, alongside a built-in electric field, with direction pointing from RP to OP [24]. Various photocatalytic materials such as graphitic carbon nitride, metal chalcogenides, metal oxides and metal nitrides have been explored to form S-scheme heterojunctions [25].

Metal sulphides such as CuS and Bi_2S_3 have been utilized as photocatalysts in wastewater treatment processes due to their small band gap energy, non-toxicity, and low cost [26–29]. However, they suffer high charge carrier recombination that limits their application in photocatalytic processes. Similarly, graphitic carbon nitride (g-C_3N_4), which is a visible light active carbon material have enjoyed much attention in recent years [30,31]. Its photocatalytic activity is also limited by high charge carrier recombination. Therefore, in this study S-scheme g-C_3N_4/Bi_2S_3/CuS heterostructures have been synthesized through a facile solvothermal process to study the potential synergy among the materials in the photocatalytic degradation of MO. The degradation experiment revealed a significant increase in the photocatalytic activity of the heterostructures compared to the pristine CuS, Bi_2S_3 and g-C_3N_4. This study shows the potential of achieving increased photocatalytic activity by creating heterostructures with semiconductor materials, which mitigates their limitations.

2. Experimental

2.1. Materials and methods

Bismuth nitrate(III) pentahydrate [$Bi(NO_3)_3{\cdot}5H_2O$], copper(II) nitrate hemi-pentahydrate [$Cu(NO_3)_2){\bullet}2.5H_2O$], melamine ($C_3H_6N_6$), ethylene glycol (EG), dodecanethiol-1 (DDT), N-alkyl aniline, ammonia (NH_3), carbon disulphide (CS_2), and ethanol (C_2H_5OH) were supplied by Merck pty South Africa.

2.2. Characterization of g-C_3N_4/Bi_2S_3/CuS

Structural properties of the nanomaterials were studied using powder X-ray diffraction (XRD), which was recorded on a Bruker D8 Advanced machine equipped with a proportional counter using Cu Kαradiation (λ = 1.5405 A, nickel filter). The morphology of the nanoparticles was studied using scanning electron microscopy and transmission electron microscopy (Hitachi HF–2000 TEM at 200 kV and FEI Tecnai G2 Twin at 20 kV). The optical properties of the materials were studied using absorption and emission spectroscopy. Absorption spectroscopy was measured using a variant UV–vis spectrophotometer. For emission spectroscopy, a Perkin Elmer LS 45 Fluorimeter was employed.

2.3. Synthesis of g-C_3N_4, CuS and Bi_2S_3

The method employed for the synthesis of g-C_3N_4 and Bi_2S_3 was earlier reported by Onwudiwe, *et al.* [32]. For the synthesis of CuS, the single source precursor method using copper(II) dithiocarbamate complex as precursor was employed. Full details of the synthesis procedures are discussed in supplementary file, S1.

2.4. Synthesis of g-C_3N_4/Bi_2S_3/CuS

Solvothermal technique was employed for the synthesis of the ternary heterostructure. In a typical synthesis, g-C_3N_4 and Bi_2S_3 were dispersed in ethylene glycol in ratio 1:1, and the mixture was transferred into an autoclave, and heated at 180 °C for 24 h. The obtained g-C_3N_4/Bi_2S_3 was washed several times with ethanol and dried under vacuum. For the synthesis of g-C_3N_4/Bi_2S_3/CuS, the obtained g-C_3N_4/Bi_2S_3 was dispersed in ethylene glycol with varied ratio of CuS, to obtain weight percentage of 5, 10, and 20% of CuS. The mixture was transferred into an autoclave and heated for 24 h at 180 °C. The obtained ternary heterostructure was washed several times with ethanol and then dried under vacuum.

2.5. Photocatalytic degradation studies

The photocatalytic activity of the photocatalysts was evaluated using methyl orange as the test pollutant under visible light irradiation. In a typical process, 100 mL of 0.1 mg/L MO was measured into a beaker. Afterwards, 10 mg of the catalyst was added into the solution and stirred for 30 min to achieve adsorption and desorption equilibrium. Subsequently, the mixture was irradiated under visible light and aliquots were

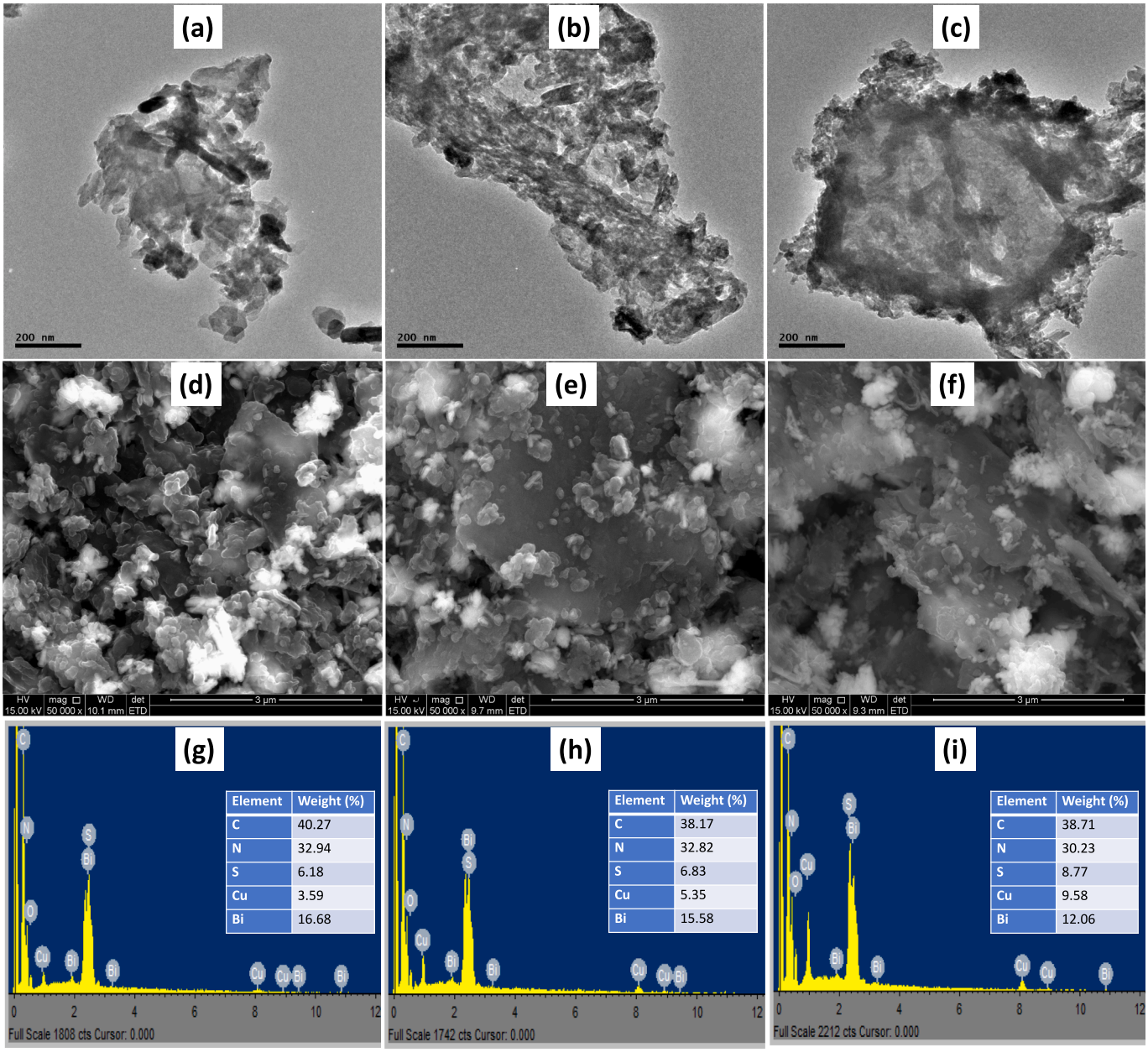

Fig. 2. TEM (a-c), SEM (d-f), and EDX (g-i) of GCN-BiS/CuS at 5, 10, and 20% of CuS loading respectively.

taken from the sample at regular intervals. The percentage degradation of MO after 60 min was calculated using equation (1),

$$\%degradation = \frac{A_o - A_t}{A_o} \times 100 \quad (1)$$

where A_o and A_t are the initial and final absorbance of the solution respectively. The degradation data for the process was fitted into the linear form of the pseudo first order kinetics to evaluate the reaction rate constant for the process using equation (2),

$$\ln(C_t) = \ln(C_o) - kt \quad (2)$$

where C_o and C_t represent the initial and final concentrations of the solution after time t respectively, and k represents the reaction rate constant.

3. Results and discussion

3.1. Structural and morphological studies

The XRD patterns of GCN, CuS, Bi_2S_3 and GCN/Bi_2S_3/CuS heterostructures are shown in Fig. 1. The diffraction pattern of GCN showed a distinct peak at 28°, which is ascribed to the 002 planes arising from the interlayer stacking of the graphitic-like structure [33]. In the CuS sample, the pattern could be indexed to the hexagonal phase of CuS (JCPDS No. 78-0876) [34], while the diffraction pattern of Bi_2S_3 showed peaks that matched the primitive orthorhombic phase of Bi_2S_3 (JCPDS No. 170320) with Pbnm space group [35]. The diffraction pattern for GCN/Bi_2S_3 exhibited diffraction peaks due to both GCN and Bi_2S_3, indicating that the structures of both materials were maintained after compositing. However, a slight reduction in the intensity of the peaks of BiS is noticeable, which indicates a reduction in the crystallinity of the Bi_2S_3.

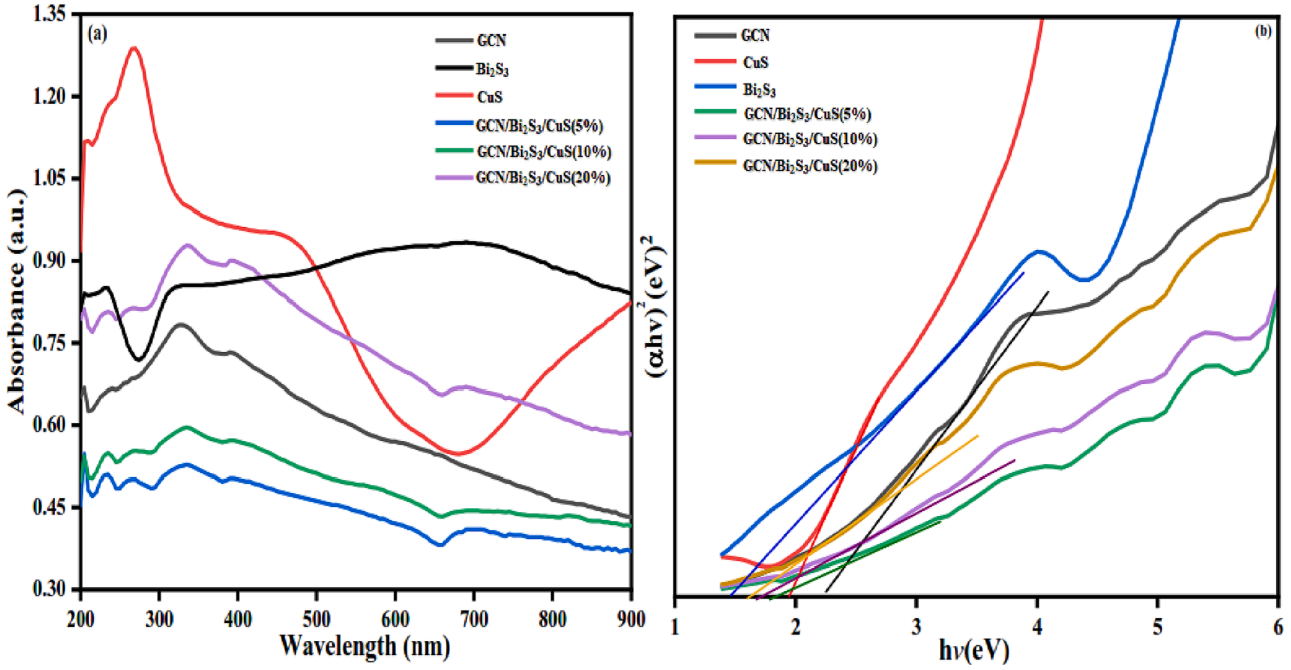

Fig. 3. UV–visible spectra of (a) g-C_3N_4, Bi_2S_3, CuS, GCN/Bi_2S_3/CuS(5%), GCN/Bi_2S_3/CuS(10%) and GCN/Bi_2S_3/CuS(20%) and (b) Tauc plot obtained from absorption spectra.

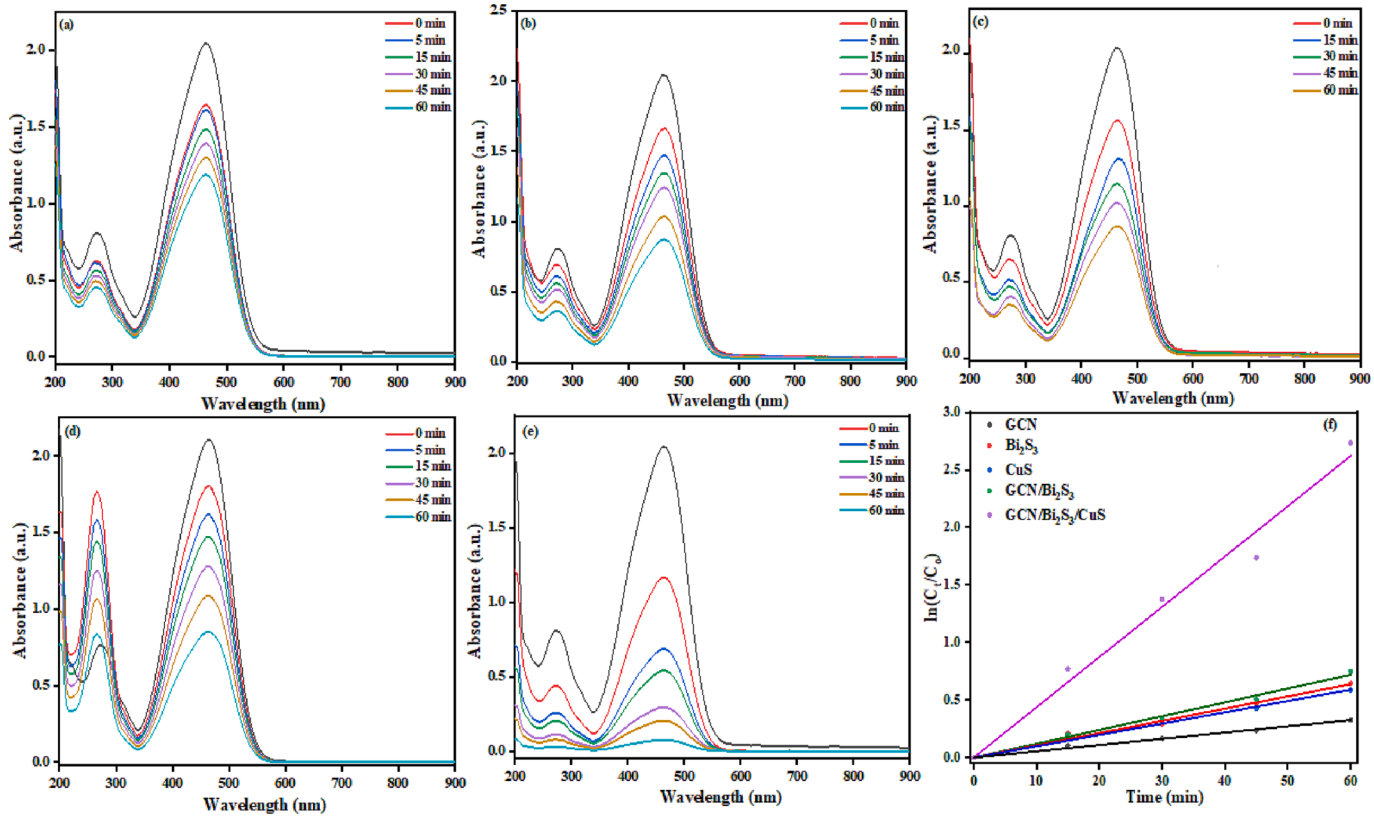

Fig. 4. Degradation profile of (a) GCN, (b) CuS, (c) Bi_2S_3, (d) GCN/Bi_2S_3 and (e) GCN/Bi_2S_3/CuS composite for methyl orange and (f) pseudo first order kinetic plot for the degradation profile of methyl orange by GCN, CuS, Bi_2S_3, GCN/Bi_2S_3 and GCN/Bi_2S_3/CuS.

The ternary GCN/Bi_2S_3/CuS composites showed a gradual increase in the CuS peak at 49°, which confirms an increase in the amount of CuS in the composite.

The SEM and TEM images of GCN, CuS, and Bi_2S_3, are presented in Figs. S1-S3 of the supplementary document, which show that they are composed of rod-shaped particles. Fig. 2a, b and c are the TEM micrographs of GCN/Bi_2S_3/CuS(5%), GCN/Bi_2S_3/CuS(10%), and GCN/Bi_2S_3/CuS(20%) respectively. The layered structures of GCN sheets are

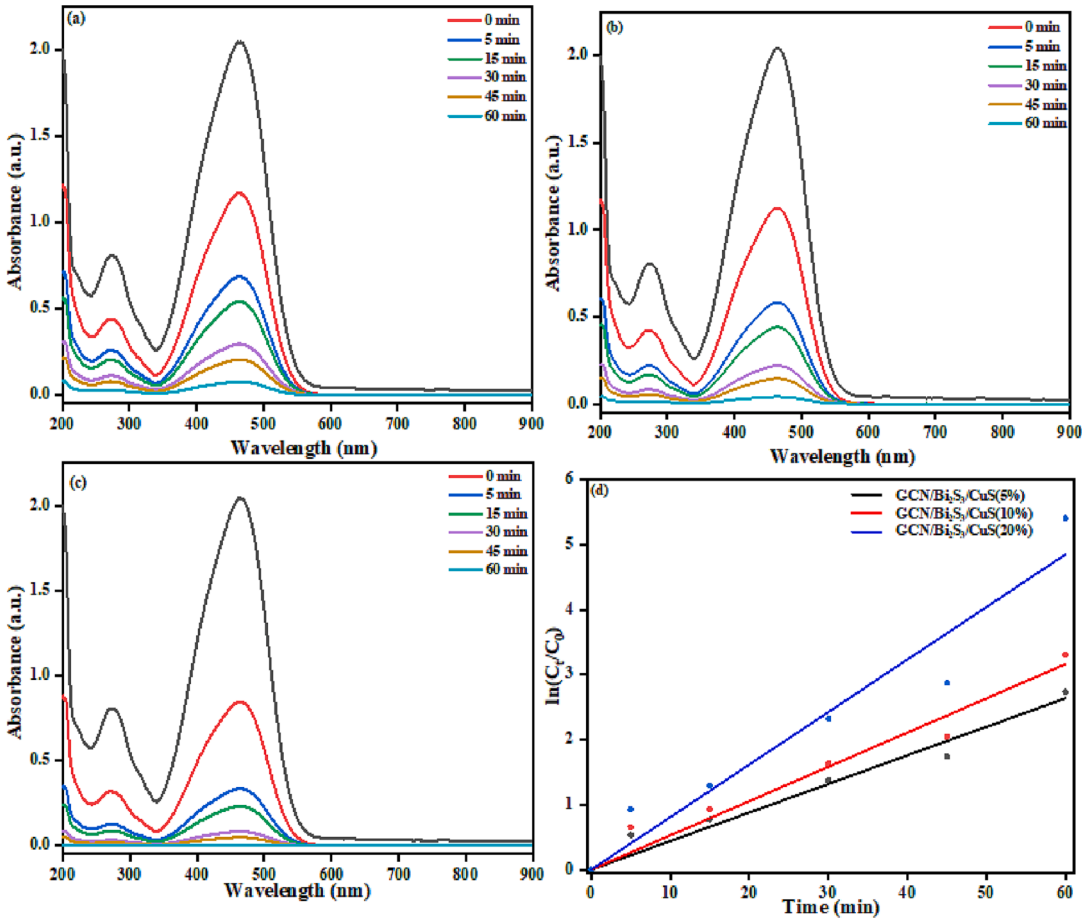

Fig. 5. Effect of percentage composition of CuS on the photocatalytic activity of GCN/BiS/CuS(5%), GCN/BiS/CuS(10%) and GCN/BiS/CuS(20%).

noticeable at the different concentration of the CuS. SEM measurement presents a better image of GCN because of its advantage in scanning the surface morphology and detecting the layers, folds, and discontinuities within the structure of the 2D material. The SEM images of the GCN/Bi_2S_3/CuS composites (Fig. 2d -f) also showed the deposition of the nanoparticles on the g-C_3N_4 surface. With increase in the percentage composition of CuS, the images became darker, showing the presence of higher amount of the nanoparticles. The EDX spectra of the composites (Fig. 2g – i) also confirmed the successful formation of the GCN/Bi_2S_3/CuS composite, and the percentage of the elemental composition (in the inset) showed proportional increase in the percentage of Cu and S that conforms with the increase in the amount of CuS loading in the nanocomposite.

3.2. Optical properties studies

The absorption spectra of GCN, Bi_2S_3, CuS and GCN /Bi_2S_3/CuS composites are shown in Fig. 3. GCN showed a relatively strong absorption in the visible range of the spectrum which tails into the near-infrared region with an absorption edge around 550 nm. The CuS nanoparticles exhibited the highest absorption intensity in the visible region and showed increasing absorption into the near-infrared. Moreover, the absorption edge of the CuS was around 380 nm. In the spectrum of the GCN/Bi_2S_3/CuS composites, the absorption intensity was observed to increase with the percentage composition of CuS, showing improved light absorption. Also, the band edge of the composite was red-shifted with increase in CuS composition. The calculated band gap energy for GCN, Bi_2S_3 and CuS was 2.25, 1.47 and 1.95 eV respectively, which agrees with literature reports [36–38]. A narrowing of the band gap energy occurred in the GCN/Bi_2S_3/CuS composites as the percentage of CuS increased. The band gap was 1.79, 1.73 and 1.60 eV for GCN/Bi_2S_3/CuS(5%), GCN/Bi_2S_3/CuS(10%) and GCN/Bi_2S_3/CuS(20%) respectively. This reduction in band gap energy could be ascribed to the formation of heterostructures between GCN, Bi_2S_3, and CuS. The narrowing of the band gap could be significant for enhancing the photocatalytic activity of the composites, as it could potentially improve charge carrier generation of the material [39].

3.3. Photodegradation studies of the binary nanomaterials and composites

The degradation profile of GCN, CuS, Bi_2S_3, GCN/Bi_2S_3, and GCN/Bi_2S_3/CuS(5%) for methyl orange is presented in Fig. 4. GCN, CuS and Bi_2S_3 showed 40, 55, and 57% degradation efficiency, as shown in Fig. 4a, b and c, respectively. The compositing of GCN with Bi_2S_3 to form GCN/Bi_2S_3 composite resulted in an increase of the degradation efficiency to 75% (Fig. 4d) indicating an enhancement of charge carrier generation and separation. After the introduction of CuS into the composite to form GCN/Bi_2S_3/CuS(5%), the photocatalytic degradation of methyl orange reached 98% (Fig. 4e). The improved photocatalytic activity of the ternary composite could be attributed to the formation of heterostructure at the interface of the materials. This could result in improved charge separation compared to the other materials. The pseudo-first rate constant for the degradation was 5.0×10^{-3}, 1.1×10^{-2}, 1.2×10^{-2}, 1.5×10^{-2}, 4.4×10^{-2} min^{-1} for GCN, CuS, Bi_2S_3, GCN/Bi_2S_3 and GCN/Bi_2S_3/CuS(5%) respectively (Fig. 4f).

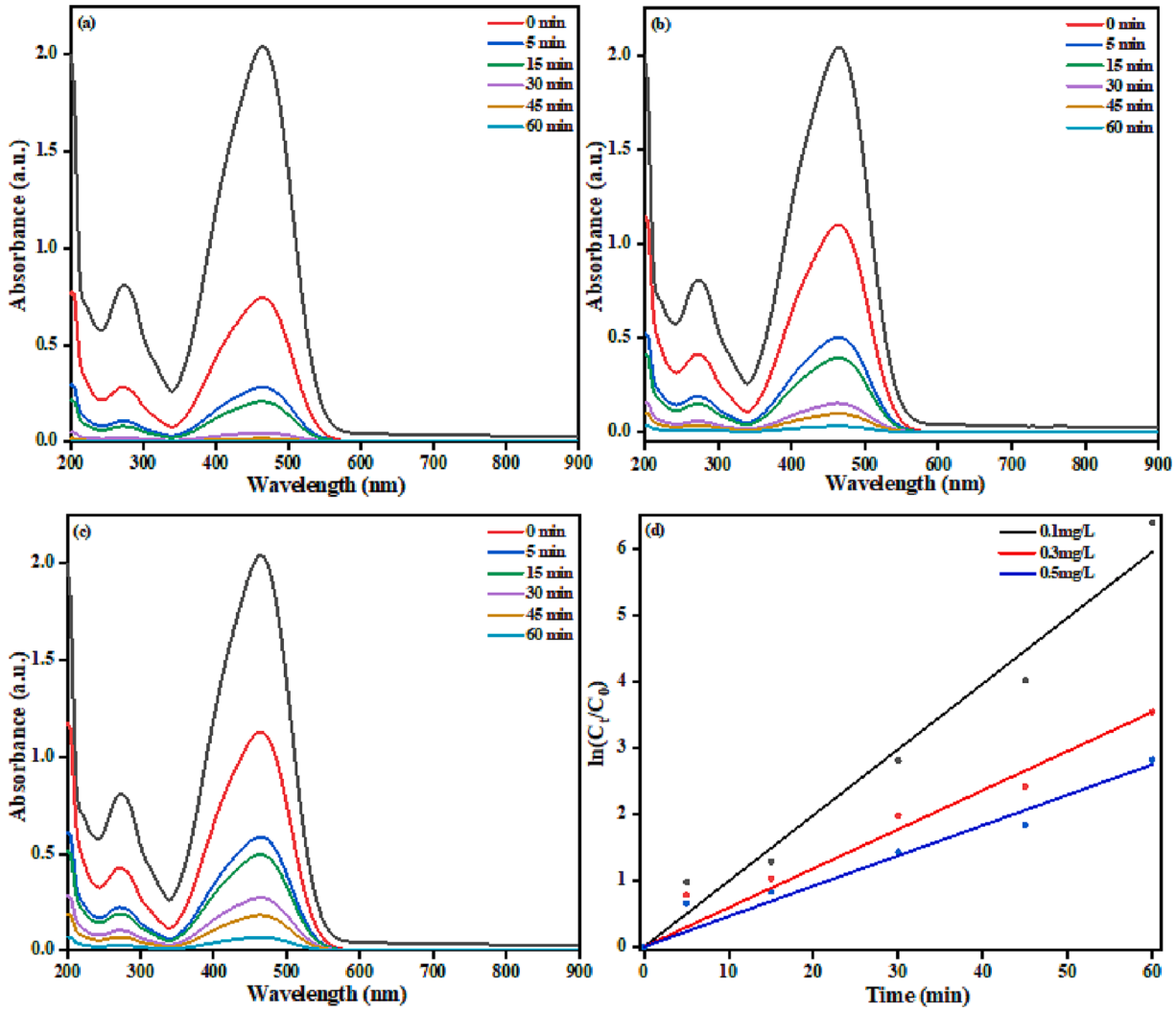

Fig. 6. Effect of dye concentration at (a) 0.1 mg/L, (b) 0.3 mg/L and (c) 0.5 mg/L on the photocatalytic degradation of methylene blue and (d) the kinetic plots for the effect of dye concentration on the photocatalytic degradation of methyl orange.

3.4. Effect of process parameters

The effect of percentage composition of CuS on the photocatalytic activity of the catalyst is shown in Fig. 5. An increase in the degradation efficiency of the catalyst was observed with increase in the ratio of CuS in the composite. GCN/Bi_2S_3/CuS(5%), GCN/Bi_2S_3/CuS(10%) and GCN/Bi_2S_3/CuS(20%) achieved 98, 100, and 100% degradation efficiency (Fig. 5a, b and c respectively) with a corresponding k values of 4.40×10^{-2}. 5.30×10^{-2}, and 8.10×10^{-2} min^{-1} respectively (Fig. 5d). The increase in k at higher percentage composition of CuS, is indicative of a faster reaction rate, due to higher active sites on the heterostructure and improved charge carrier generation due to lowered band gap energy. This ability of CuS to enhance degradation process was similarly reported when it was incorporated into ZnO for photocatalytic degradation of methylene blue dye [40].

The ternary GCN/Bi_2S_3/CuS catalyst showed efficient photocatalytic activity for the dye degradation in the concentration range of 0.1 – 0.5 mg/L as shown in Fig. 6. The degradation efficiency of MO reached 100, 100, and 98% at 0.1, 0.3 and 0.5 mg/L in Fig. 6a, b and c respectively. The sustenance of the high catalytic activity of the catalyst even at increased dye concentration confirmed the effectiveness of the ternary heterostructure for MO degradation. The pseudo first order rate constant for the degradation was 9.90×10^{-2}, 5.90×10^{-2}, and 4.60×10^{-2} min^{-1} respectively (Fig. 6d).

As shown in Fig. 7, the ternary heterostructure exhibited high catalytic efficiency across the evaluated pH range of 3–10. No significant reduction in the activity of the catalyst was observed under acidic, neutral, and basic conditions. The solution pH often influences the ionic state of a specie in solution and, the nature of charge on the surface of a material [41]. Therefore, it could significantly influence the interaction between the MO molecule and the catalytic material. The effectiveness of the catalyst across the pH range, showed its potential for application in a wide range of wastewater matrix.

3.5. Radical scavenging studies

To understand the mechanism of action of the ternary heterostructure, radical scavenging experiments were carried out by introducing radical scavengers into the system. Ascorbic acid (ASC), silver nitrate (SN), *tert*-butanol (TBA) and triethylamine (TEA) were added as $O_2^{\cdot-}$, e^-, $^{\cdot}OH$, and h^+ scavengers. Fig. 8a shows that TBA had the most significant effect on the degradation efficiency of the process resulting in 50% reduction. TEA and SN both resulted in about 35 and 30% reduction, respectively. This implies that $^{\cdot}OH$ radical had the most influence on the degradation process. The kinetics of the radial scavenging process followed a Pseudo first order kinetics as shown in Fig. 8b.

The mechanism of radical generation in the ternary heterostructure was explored by studying the band alignment through the calculations

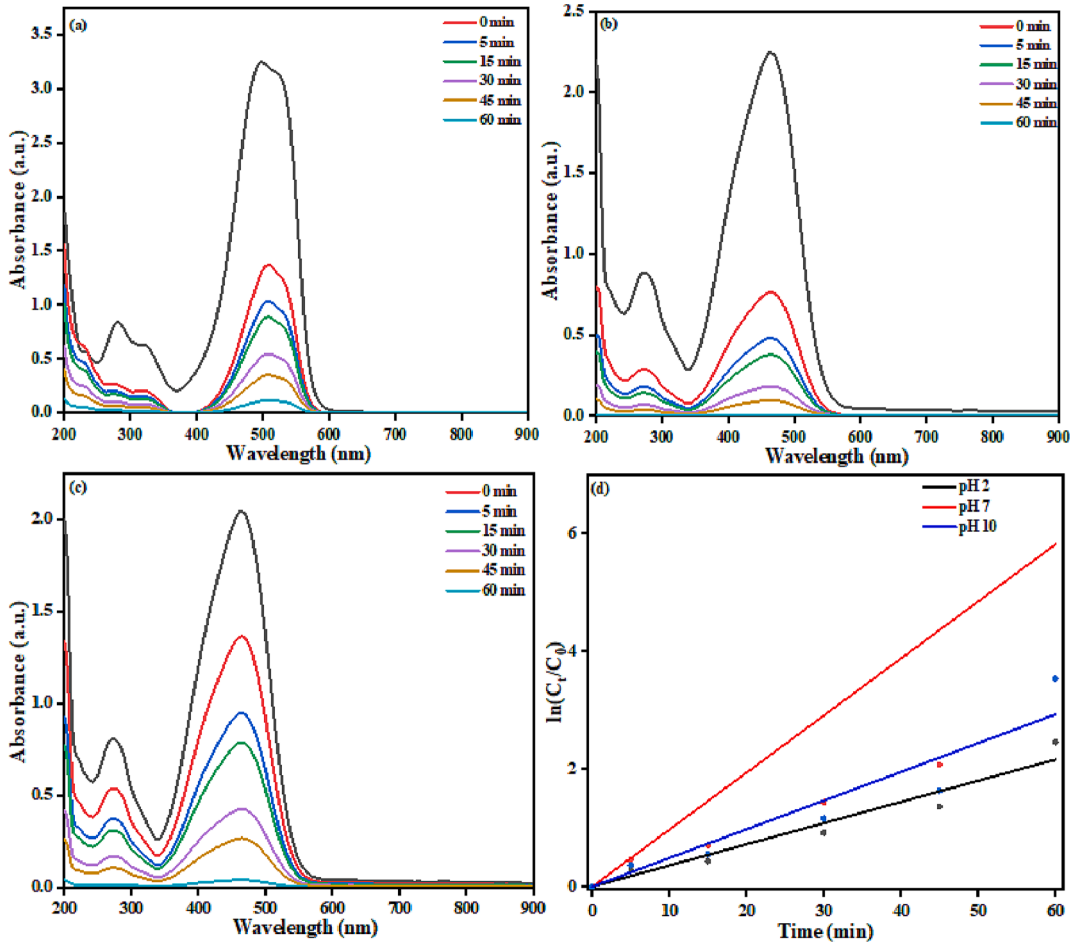

Fig. 7. Photocatalytic degradation profile of MO at pH of (a) 2, (b) 7, (c) 10 and (d) pseudo first order kinetics for the degradation of MO at pH 2, 7 and 10.

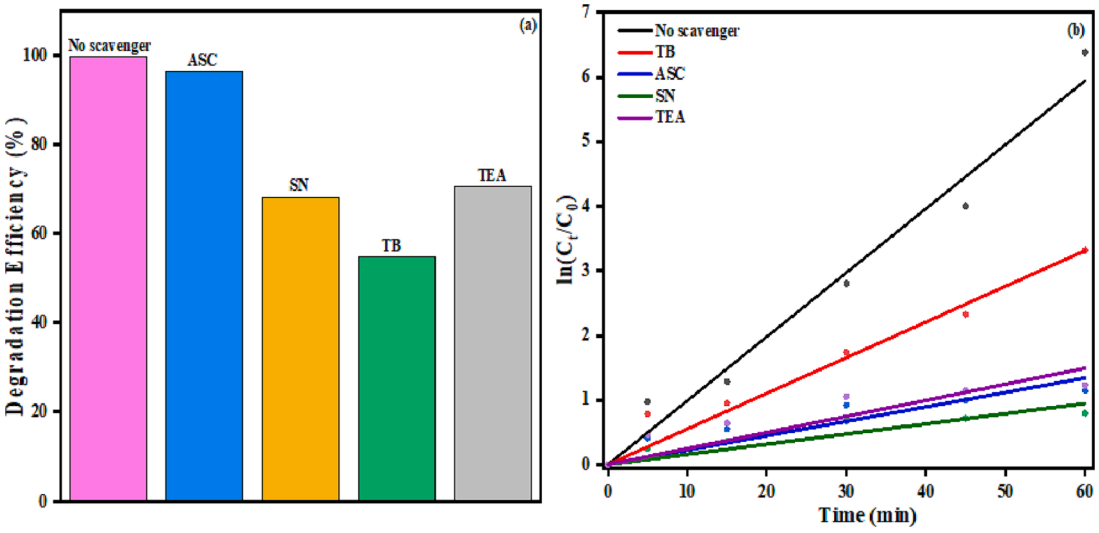

Fig. 8. Radical scavenging studies for methyl orange (a) in the presence of TB, TEA, SN, ASC and (b) Pseudo first order kinetics for the radial scavenging experiments.

Table 1
Calculated band alignment for GCN, Bi_2S_3, and CuS.

Semiconductor	E_{CB}	E_{VB}
GCN	−0.98	1.27
Bi_2S_3	0.035	1.51
CuS	−0.185	1.77

involving the empirical data and equations (3) and (4):

$$E_{CB} = X - E_e - \frac{1}{2}E_g \quad (3)$$

$$E_{VB} = E_{CB} + E_g \quad (4)$$

where X is the Mulliken's electronegativity, E_e is the energy of free electrons on the hydrogen scale, E_{CB} is the conduction band potential, E_{VB} is the valence band potential, and E_g is the band gap energy. The value of E_e is 4.5 eV, while *X* for GCN, Bi_2S_3 and CuS are 4.64, 5.27 and 5.29 eV respectively. The calculated band alignments are shown in Table 1 and the E_{VB} of the semiconductors were less positive compared to the $OH^-/{}^{\cdot}OH$ and are not capable of generating ${}^{\cdot}OH$. The radical scavenging experiment confirmed ${}^{\cdot}OH$ as the most significant radical in the degradation process, which suggests its formation through a different route in the reaction process. Since the E_{CB} of Bi_2S_3 is less positive than the O_2/H_2O_2 potential, the adsorbed O_2 may react directly with photogenerated electrons to produce H_2O_2, which further reacts with electrons to produce ${}^{\cdot}OH$ as shown in equations (5) and (6) [42–44],

$$O_2 + 2H^+ + 2e^- \rightarrow H_2O_2 \quad (5)$$

$$H_2O_2 + e^- \rightarrow {}^{\cdot} + OH^- \quad (6)$$

The overall mechanism of the MO degradation is presented in Fig. 9 (a). The high work function (4.93 eV) [45] and electron capture ability of Bi_2S_3, implies that it can capture photogenerated electrons by the GCN/Bi_2S_3 structure, while the photogenerated electrons on Bi_2S_3 electrons could then react with adsorbed O_2 on the catalyst surface. After the incorporation of CuS, under visible light, GCN and CuS could form a heterostructure with staggered band structure to produce electron-hole pairs. The reported work function for CuS and GCN are 4.95 and 4.00 eV respectively [46,47], so the Fermi energy (E_F) of CuS is lower than that of GCN. When GCN and CuS are in contact, a flow of electron from the semiconductor with a high E_F to that with a low EF is observed, leading to the generation of a built-in electric field (IEF) from GCN to CuS at the GCN/CuS interface. This IEF leads to the recombination of the oxidizing holes in GCN with electrons in the conduction band of CuS, resulting in an enhancement of photogenerated charge carriers in GCN/Bi_2S_3/CuS photocatalyst. This shows a S-scheme heterojunction path for charge transport and separation in the GCN/Bi_2S_3/CuS heterostructure [24,48]. The holes in the E_{VB} of CuS could also migrate to the surface to induce direct oxidation of MO [49]. Fig. 9(b) shows the PL spectra of GCN/Bi_2S_3/CuS and GCN, which confirms the enhanced charge carrier separation in the heterostructure compared to pristine GCN.

4. Conclusion

The synthesis of a photocatalytically active dual heterostructure semiconductor was successfully achieved through a facile solvothermal process. The constructed heterostructure obtained from g-C_3N_4, CuS and Bi_2S_3 promises effective light absorption property which could be modified by varying the composition of the material. Compared to g-C_3N_4, the g-C_3N_4/Bi_2S_3/CuS heterostructure showed significant fluorescence quenching, which is indicative of improved charge separation. The ternary nanocomposite showed high photocatalytic performance for methyl orange degradation, achieving 98% degradation and a reaction rate constant of 8.10×10^{-2} min^{-1}. The enhanced photocatalytic activity of the heterostructure could be ascribed to the band alignment of the semiconductors, which allows for the transfer of photogenerated electrons into the Bi_2S_3 CB, while photogenerated holes are accumulated in the VB of g-C_3N_4. This minimizes the chances of charge carrier recombination and the subsequent degradation of MO molecules. These results show the potential of this heterostructure to be explored in practical application for wastewater treatment.

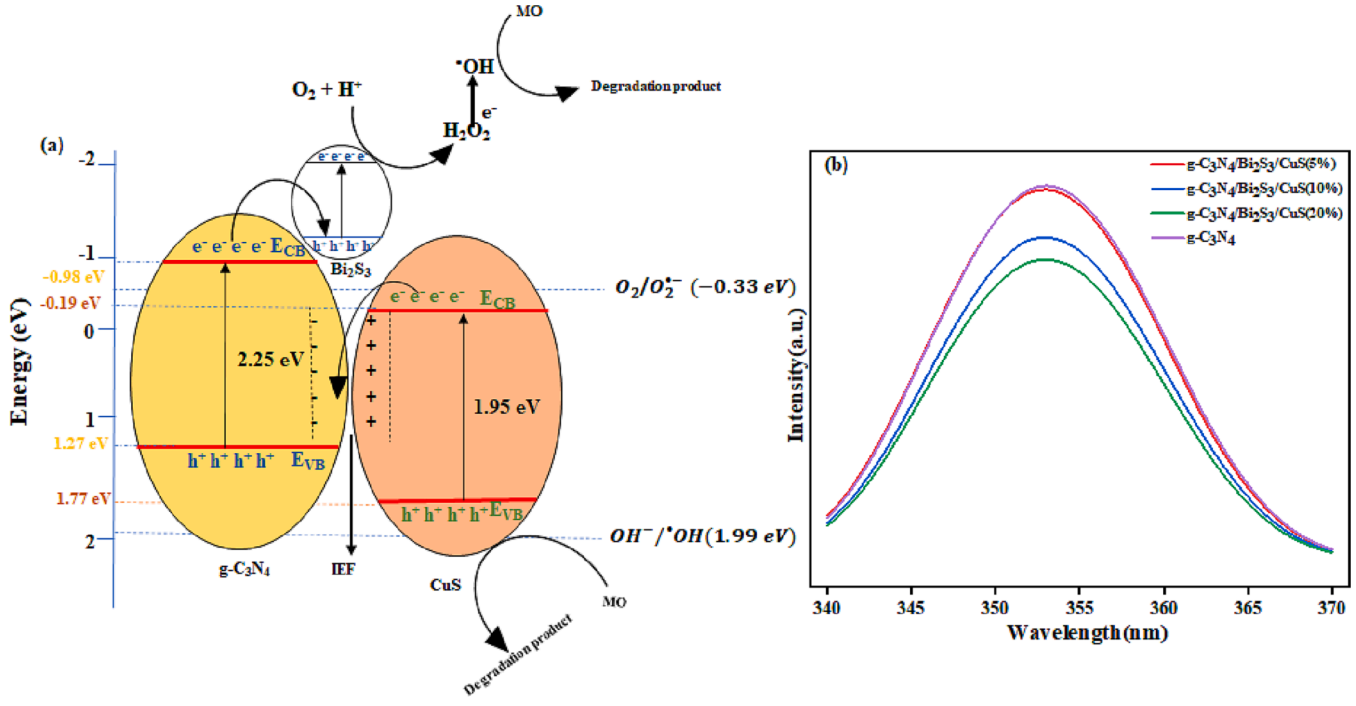

Fig. 9. (a) Mechanism of radical generation by GCN/Bi_2S_3/CuS and (b) PL spectra of GCN, GCN/Bi_2S_3/CuS(5%), GCN/Bi_2S_3/CuS(10%) and GCN/Bi_2S_3/CuS(20%).

Declaration of Competing Interest

The authors declare that they have no known competing financial interests or personal relationships that could have appeared to influence the work reported in this paper.

Data availability

Data will be made available on request.

Acknowledgement

The Authors gratefully acknowledge the Finacial support from the North-West University, South Africa (grants ref: 1K02799).

Appendix A. Supplementary material

Supplementary data to this article can be found online at https://doi.org/10.1016/j.inoche.2023.111075.

References

[1] J. Adeleke, T. Theivasanthi, M. Thiruppathi, M. Swaminathan, T. Akomolafe, A. Alabi, Photocatalytic degradation of methylene blue by ZnO/NiFe2O4 nanoparticles, Appl. Surf. Sci. 455 (2018) 195–200.
[2] K. Atrak, A. Ramazani, S.T. Fardood, Eco-friendly synthesis of Mg0. 5Ni0. 5AlxFe2-xO4 magnetic nanoparticles and study of their photocatalytic activity for degradation of direct blue 129 dye, J. Photochem. Photobiol. A Chem. 382 (2019), 111942.
[3] H.A.H. Alzahrani, Y.Q. Almulaiky, A.O. Alsaiari, The photocatalytic dye degradation of methylene blue (MB) by nanostructured ZnO under UV irradiation, Phys. Scr. 98 (2023), 045703.
[4] R.H. Waghchaure, V.A. Adole, B.S. Jagdale, Photocatalytic degradation of methylene blue, rhodamine B, methyl orange and Eriochrome black T dyes by modified ZnO nanocatalysts: A concise review, Inorg. Chem. Commun. 143 (2022), 109764.
[5] S.H.S. Chan, T. Yeong Wu, J.C. Juan, C.Y. Teh, Recent developments of metal oxide semiconductors as photocatalysts in advanced oxidation processes (AOPs) for treatment of dye waste-water, J. Chem. Technol. Biotechnol. 86 (2011) 1130–1158.
[6] A. Kulis-Kapuscinska, M. Kwoka, M.A. Borysiewicz, T. Wojciechowski, N. Licciardello, M. Sgarzi, G. Cuniberti, Photocatalytic degradation of methylene blue at nanostructured ZnO thin films, Nanotechnology 34 (2023), 155702.
[7] S. Alwera, V.S. Talismanov, V. Alwera, D. Domyati, Synthesis and Characterization of Sn-Doped CeO2-Fe2O3 Nanocomposite and Application in Photocatalytic Degradation of Sudan I, Biointerface Res. Appl. Chem. 13 (2023).
[8] S.J. Phang, V.L. Wong, K.H. Cheah, L.L. Tan, Robust graphitic carbon nitrite-based thermoset coating for synergistic adsorption-photocatalysis process in 3D-printed photoreactors, Energy Rep. 9 (2023) 30–37.
[9] S. Mishra, S. Soren, A.K. Debnath, K. Muthe, N. Das, P. Parhi, Microwave-mediated One-step Synthesis of CeVO4-rGO Composites with Enhanced Photocatalytic Activity under Visible Light, ChemistrySelect 8 (2023).
[10] R. Stanley, S.K. Balu, J.A. Jebasingh, S.M. Vidyavathy, Super-efficient photocatalytic degradation of methylene blue, methyl orange and rhodamine B dyes using low-cost ZnO-MgO nanocomposite under natural sunlight and its bactericidal activity, Res. Chem. Intermediates.
[11] H. Liyanaarachchi, C. Thambiliyagodage, C. Liyanaarachchi, U. Samarakoon, Efficient photocatalysis of Cu doped TiO2/g-C3N4 for the photodegradation of methylene blue, Arab. J. Chem. 16 (2023).
[12] J. Gaur, K. Vikrant, K.H. Kim, S. Kumar, M. Pal, R. Badru, S. Masand, J. Momoh, Photocatalytic degradation of Congo red dye using zinc oxide nanoparticles prepared using Carica papaya leaf extract, Mater. Today Sustain. 22 (2023), 100339.
[13] U. Abdullah, M. Ali, E. Pervaiz, An Inclusive Review on Recent Advancements of Cadmium Sulfide Nanostructures and its Hybrids for Photocatalytic and Electrocatalytic Applications, Mol. Catal. 508 (2021).
[14] D. Bury, M. Jakubczak, M.A.K. Purbayanto, A. Wojciechowska, D. Moszczyńska, A. M. Jastrzębska, Photocatalytic Activity of the Oxidation Stabilized Ti3C2Tx MXene in Decomposing Methylene Blue, Bromocresol Green and Commercial Textile Dye, Small, Methods n/a (2023) 2201252.
[15] D. Tilgner, M. Friedrich, A. Verch, N. de Jonge, R. Kempe, A Metal-Organic Framework Supported Nonprecious Metal Photocatalyst for Visible-Light-Driven Wastewater Treatment, ChemPhotoChem 2 (2018) 349–352.
[16] E.S. Mansor, F.N. El Shall, E.K. Radwan, Simultaneous decolorization of anionic and cationic dyes by 3D metal-free easily separable visible light active photocatalyst, Environ. Sci. Pollut. Res.
[17] U. Rafiq, O. Mehraj, S. Lone, M. Wahid, K. Majid, Solvothermal synthesis of Ag2WO4/Sb2WO6 heterostructures for enhanced charge transfer properties and efficient visible-light-driven photocatalytic activity and stability, J. Environ. Chem. Eng. 8 (2020), 104301.
[18] L. Qiu, Y. Wang, X. Zhang, F. Tian, C. Zhu, J. Sheng, W. Yang, Y. Yu, ZnS Nanospheres Coated with ZnSe/MoSe2 Shells as Dual Heterojunctions with Wide Spectral Responses for the Photoreduction of Cr(VI), ACS Appl. Nano Mater. 6 (2023) 523–532.
[19] P.J. Mafa, M.E. Malefane, A.O. Idris, B.B. Mamba, D. Liu, J. Gui, A.T. Kuvarega, Cobalt oxide/copper bismuth oxide/samarium vanadate (Co3O4/CuBi2O4/SmVO4) dual Z-scheme heterostructured photocatalyst with high charge-transfer efficiency: Enhanced carbamazepine degradation under visible light irradiation, J. Colloid Interface Sci. 603 (2021) 666–684.
[20] Q. Xu, S. Wageh, A.A. Al-Ghamdi, X. Li, Design principle of S-scheme heterojunction photocatalyst, J. Mater. Sci. Technol. 124 (2022) 171–173.
[21] L. Zhang, Q. Shen, F. Huang, L. Jiang, J. Liu, J. Sheng, Y. Li, H. Yang, Electrospinning directly synthesis of 0D/1D CuBi2O4@WO3 nanofiber photocatalyst with S-scheme heterojunction, Appl. Surf. Sci. 608 (2023), 155064.
[22] X. Dou, Y. Chen, H. Shi, CuBi2O4/BiOBr composites promoted PMS activation for the degradation of tetracycline: S-scheme mechanism boosted Cu2+/Cu+ cycle, Chem. Eng. J. 431 (2022), 134054.
[23] F. Mei, K. Dai, J. Zhang, W. Li, C. Liang, Construction of Ag SPR-promoted step-scheme porous g-C3N4/Ag3VO4 heterojunction for improving photocatalytic activity, Appl. Surf. Sci. 488 (2019) 151–160.
[24] L. Zhang, J. Zhang, H. Yu, J. Yu, Emerging S-Scheme Photocatalyst, Adv. Mater. 34 (2022) 2107668.
[25] L. Wang, B. Zhu, J. Zhang, J.B. Ghasemi, M. Mousavi, J. Yu, S-scheme heterojunction photocatalysts for CO2 reduction, Matter 5 (2022) 4187–4211.
[26] L. Isac, C. Cazan, L. Andronic, A. Enesca, CuS-Based Nanostructures as Catalysts for Organic Pollutants Photodegradation, in: Catalysts, 2022.
[27] T. Cai, Y. Ding, L. Xu, Synthesis of flower-like CuS/graphene aerogels for dye wastewater treatment, Funct. Mater. Lett. 12 (2018) 1950002.
[28] Y.-H. Li, Z. Wang, Green synthesis of multifunctional copper sulfide for efficient adsorption and photocatalysis, Chem. Pap. 73 (2019) 2297–2308.
[29] L. Luo, X. Shen, L. Song, Y. Zhang, B. Zhu, J. Liu, Q. Chen, Z. Chen, L. Zhang, MoS2/Bi2S3 heterojunctions-decorated carbon-fiber cloth as flexible and filter-membrane-shaped photocatalyst for the efficient degradation of flowing wastewater, J. Alloy. Compd. 779 (2019) 599–608.
[30] X. Zhang, H. Zhang, P. Chen, M. Liu, P. Wu, C. Liu, W. Jiang, One-step dye wastewater treatment by combined adsorption, extraction, and photocatalysis using g-C3N4 pickering emulsion, Colloids Surf. A Physicochem. Eng. Asp 644 (2022), 128814.
[31] N. Ding, X. Chang, N. Shi, X. Yin, F. Qi, Y. Sun, Enhanced inactivation of antibiotic-resistant bacteria isolated from secondary effluents by g-C3N4 photocatalysis, Environ. Sci. Pollut. Res. 26 (2019) 18730–18738.
[32] D.C. Onwudiwe, V.M. Nkwe, O.C. Olatunde, H. Ferjani, Graphitic carbon nitride functionalized with Cu-doped Bi2S3 as a heterostructure photocatalyst for the visible light degradation of methyl orange, Ceram. Int. (2023).
[33] H. Ding, D. Han, Y. Han, Y. Liang, X. Liu, Z. Li, S. Zhu, S. Wu, Visible light responsive CuS/ protonated g-C3N4 heterostructure for rapid sterilization, J. Hazard. Mater. 393 (2020), 122423.
[34] S. Riyaz, A. Parveen, A. Azam, Microstructural and optical properties of CuS nanoparticles prepared by sol–gel route, Perspect. Sci. 8 (2016) 632–635.
[35] A.K. Dutta, S.K. Maji, K. Mitra, A. Sarkar, N. Saha, A.B. Ghosh, B. Adhikary, Single source precursor approach to the synthesis of Bi2S3 nanoparticles: A new amperometric hydrogen peroxide biosensor, Sens. Actuators B 192 (2014) 578–585.
[36] S. Liu, J. Ke, H. Sun, J. Liu, M.O. Tade, S. Wang, Size dependence of uniformed carbon spheres in promoting graphitic carbon nitride toward enhanced photocatalysis, Appl. Catal. B 204 (2017) 358–364.
[37] P.-W. Chen, K. Li, Y.-X. Yu, W.-D. Zhang, Cobalt-doped graphitic carbon nitride photocatalysts with high activity for hydrogen evolution, Appl. Surf. Sci. 392 (2017) 608–615.
[38] M. Isik, M. Terlemezoglu, N. Gasanly, M. Parlak, Structural, morphological and temperature-tuned bandgap characteristics of CuS nano-flake thin films, Physica E 144 (2022), 115407.
[39] T. Morikawa, R. Asahi, T. Ohwaki, K. Aoki, Y. Taga, Band-Gap Narrowing of Titanium Dioxide by Nitrogen Doping, Jpn. J. Appl. Phys. 40 (2001) L561.
[40] R. Mohammed, M.E.M. Ali, E. Gomaa, M. Mohsen, Copper sulfide and zinc oxide hybrid nanocomposite for wastewater decontamination of pharmaceuticals and pesticides, Sci. Rep. 12 (2022) 18153.
[41] M.M.A. Aslam, H.-W. Kuo, W. Den, M. Sultan, K. Rasool, M. Bilal, Chapter 10 - Recent trends of carbon nanotubes and chitosan composites for hexavalent chromium removal from aqueous samples, in: S. Ahuja (Ed.), Separation Science and Technology, Academic Press, 2022, pp. 177–207.
[42] Y. Nosaka, A.Y. Nosaka, Identification and Roles of the Active Species Generated on Various Photocatalysts, in: Photocatalysis and Water Purification, 2013, pp. 1-24.
[43] M. Joy, B.N. Nair, A.A.P. Mohamed, K.G. Warrier, U.N.S. Hareesh, One-Pot Hydrothermal Synthesis of Visible-Light-Responsive MoS2/g-CNO Heterostructures for Organic-Pollutant Degradation, Eur. J. Inorg. Chem. 2016 (2016) 3912–3920.
[44] Z.H. Jabbar, A.A. Okab, B.H. Graimed, M.A. Issa, S.H. Ammar, Photocatalytic destruction of Congo red dye in wastewater using a novel Ag2WO4/Bi2S3 nanocomposite decorated g-C3N4 nanosheet as ternary S-scheme heterojunction: Improving the charge transfer efficiency, Diam. Relat. Mater. 133 (2023), 109711.

[45] Y. Zhao, X. Zhu, Y. Huang, S. Wang, J. Yang, Y. Xie, Synthesis, Growth Mechanism, and Work Function at Highly Oriented 001 Surfaces of Bismuth Sulfide Microbelts, J. Phys. Chem. C 111 (2007) 12145–12148.
[46] M. Basu, R. Nazir, P. Fageria, S. Pande, Construction of CuS/Au Heterostructure through a Simple Photoreduction Route for Enhanced Electrochemical Hydrogen Evolution and Photocatalysis, Sci. Rep. 6 (2016) 34738.
[47] F. Yang, M. Lublow, S. Orthmann, C. Merschjann, T. Tyborski, M. Rusu, S. Kubala, A. Thomas, R. Arrigo, M. Hävecker, T. Schedel-Niedrig, Metal-Free Photocatalytic Graphitic Carbon Nitride on p-Type Chalcopyrite as a Composite Photocathode for Light-Induced Hydrogen Evolution, ChemSusChem 5 (2012) 1227–1232.
[48] Q. Xu, L. Zhang, B. Cheng, J. Fan, J. Yu, S-Scheme Heterojunction Photocatalyst, Chem 6 (2020) 1543–1559.
[49] Y. Hong, Y. Jiang, C. Li, W. Fan, X. Yan, M. Yan, W. Shi, In-situ synthesis of direct solid-state Z-scheme V2O5/g-C3N4 heterojunctions with enhanced visible light efficiency in photocatalytic degradation of pollutants, Appl. Catal. B 180 (2016) 663–673.